Max-Planck-Institut
für Meteorologie

REPORT No. 189

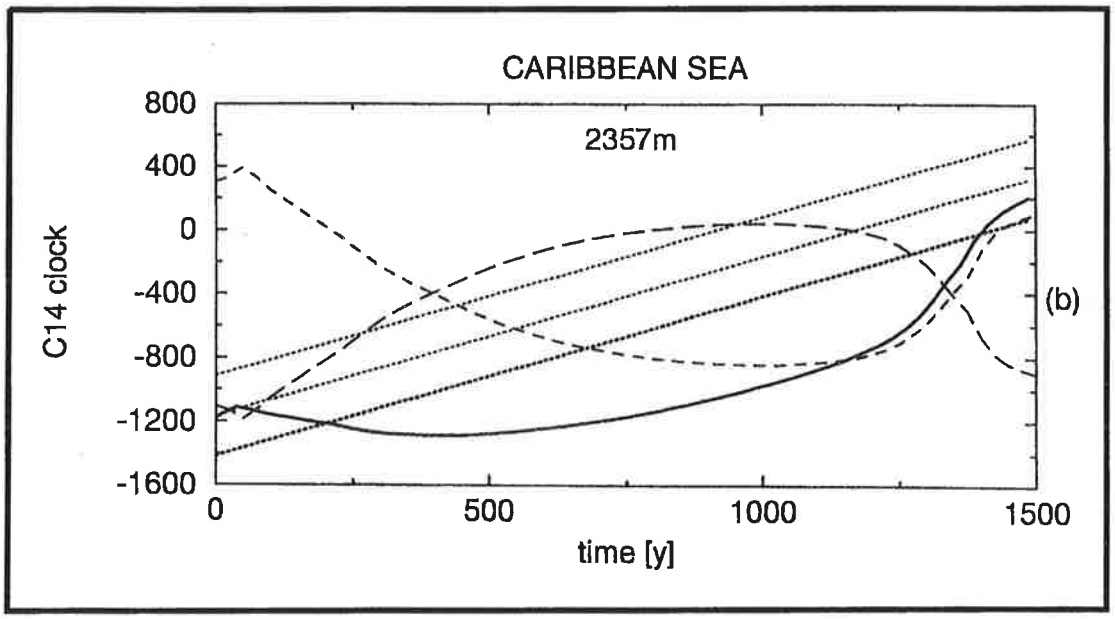

A MELTWATER INDUCED COLLAPSE OF THE ' CONVEYOR BELT ' THERMOHALINE CIRCULATION AND ITS INFLUENCE ON THE DISTRIBUTION OF Δ14C AND δ180 IN THE OCEANS

by

UWE MIKOLAJEWICZ

HAMBURG, February 1996

AUTHOR:

Uwe Mikolajewicz

Max-Planck-Institut
für Meteorologie

MAX-PLANCK-INSTITUT
FÜR METEOROLOGIE
BUNDESSTRASSE 55
D-20146 Hamburg
F.R. GERMANY

Tel.: +49-(0)40-4 11 73-0
Telefax: +49-(0)40-4 11 73-298
E-Mail: <name> @ dkrz.de

A meltwater induced collapse of the 'conveyor belt' thermohaline circulation and its influence on the distribution of Δ14C and δ18O in the oceans.

Uwe Mikolajewicz

Max-Planck-Institut für Meteorologie
Bundesstr.55
D-20146 Hamburg
FR Germany

Abstract

An ocean general circulation model coupled to a nonlinear energy balance model of the atmosphere and a statistical feedback model for wind stress shows a temporary collapse of the 'conveyor belt'-type thermohaline circulation in response to a prescribed meltwater input of 500 years duration. The thermohaline circulation of the Atlantic reverses. The associated changes in ocean heat transport lead to a strong cooling in the North Atlantic and in Europe. Due to the windstress feedback, the mode without North Atlantic deepwater formation is slightly unstable and the system slowly returns to the 'conveyor belt' overturning mode.

The circulation changes leave a strong imprint in geochemical tracers included in the model simulations. Radiocarbon chronologies are strongly affected, showing a rapidly advancing radiocarbon 'clock' when formation of North Atlantic deepwater collapses and a very slowly moving radiocarbon 'clock' when the conveyor-belt overturning starts again. In the deep Atlantic, the changes in the origin of the water masses lead to a rapid increase of the differences in radiocarbon ages relative to the surface waters. δ18O shows a similar time evolution as salinity, but the errors in the reconstruction of salinity from δ18O are typically larger than 1 psu during meltwater input. Much of the meltwater signal in sea water is obscured in carbonate shells due to the temperature effect.

ISSN 0937-1060

1. Introduction

During the past decade there have been speculations that meltwater induced changes in the thermohaline overturning of the Atlantic might be responsible for at least some of the abrupt climate changes found in geologic records (e.g. Rooth, 1982; Broecker et al., 1989). These speculations are usually based on information from two sources: Geological records such as marine sediment cores providing data about time variations of e.g. the abundance of shells of different plankton species, their geochemical composition (revealing information about geochemical composition of the sea water in which the shells were formed), and the amount and composition of material of terrestrial origin. Other important observational records are ice cores or landbased records. On the other hand, modelling studies have indicated the potential of the thermohaline circulation of the Atlantic to have multiple steady states with strongly differing oceanic heat transport at least in parts of the parameter space (e.g. Stommel, 1961; Bryan, 1986; Manabe and Stouffer, 1988). Experiments with general circulation models (GCMs) have indicated the strong effect of meltwater supply on the strength of the thermohaline overturning of the Atlantic with associated rapid changes in oceanic heat transport (e.g. Maier-Reimer and Mikolajewicz, 1989; Mikolajewicz and Maier-Reimer, 1994 for ocean-only experiments and Manabe and Stouffer, 1995 and Schiller et al., 1996 for experiments with coupled ocean atmosphere general circulation models, OAGCMs). These models integrations provide information about distributions of quantities such as temperature, salinity and sea ice, or about integral quantities like strength of the thermohaline overturning and ocean heat transport.

These two different data sets from models and geological records do not provide direct information on the same variables, but the circulation of the ocean and the distribution of temperature have an impact on the quantities measured in marine sediment cores. Thus, several methods have been developed to extract information about physical quantities of the ocean from these geological records. The relative abundance of different species gives estimates of various aspects of the seasonal cycle in sea surface temperature and sea ice coverage and hence their evolution through time (e.g. Imbrie and Kipp, 1971). Differences in radiocarbon ages between surface and deep ocean reveal information about the ventilation of the deep ocean. Other geochemical tracers like δ13C also help to reveal the position of the boundary between different water masses in the deep ocean. δ18O in the ocean (defined as the deviation of the ratio between the concentrations of the stable oxygen isotopes 18O and 16O from the average value in sea water) is influenced by several factors like e.g. the δ18O of precipitation, evaporation and the exchange between the atmosphere-ocean system with large ice sheets. An additional complication is due to the fact that the δ18O value measured in carbonate shells is not the same as in the surrounding sea water, and that the difference between these two is a function of the temperature relevant for the growth of these shells. δ18O is a good example of a frequently measured proxy index permitting various interpretations. In the last years, attempts have been made to estimate sea surface salinities, both as time series (with a resolution of a few hundred years) and as maps for certain time slices (like last glacial maximum). These methods are based on measurements of δ18O in planktonic foraminifera, temperatures reconstructed from plankton abundances and an empirical relatonship between δ18O of sea water and salinity (e.g. Duplessy et al., 1991; Duplessy et al., 1992; Wang et al., 1995).

In this paper, an attempt will be made to allow a direct comparison between model results and some quantities found in marine sediment cores. Ideal experiments to simulate the physical circulation changes for possible meltwater release scenarios should be made with a coupled OAGCM, but these models are still computationally too expensive to permit for several thousand

years of integration. Therefore, in this paper an ocean general circulation model (OGCM) coupled to a simple atmosphere model will be used for this purpose.

Two tracers which are almost independent of biological processes and are frequently measured in marine sediment cores are included in the present model; these are Δ14C and a highly idealized δ18O. A similarly simplified approach to model δ18O variations has been used in an earlier attempt with a 2.5D model by Lehman et al. (1993).

It must be stressed that the experiments presented here are highly idealized sensitivity experiments rather than attempts to reproduce the actual time variations of the oceanic circulation for any particular meltwater event. Except for the additional meltwater input, all forcing fields were left at their modern values, e.g. the only ice sheets present in the model are Antarctica and Greenland.

2. Model equations

The oceanic component of the model is the Hamburg LSG model (Maier-Reimer et al., 1993). The horizontal resolution is $3.5 \times 3.5^{\circ}$ on an E-type grid (Arakawa and Lamb, 1977). The present version has an increased vertical resolution. The thicknesses of the 22 layers increase with depth, starting with a thickness of 50 m at the surface. The thickness increases by approximately 14% per level, leading to a thickness of the lowest layer of 738 m.

The model is based on the standard set of equations (Navier-Stokes, continuity, conservation of heat, salt and sea ice) together with the standard set of simplifications (Boussinesq and hydrostatic assumption, incompressibility). The only nonstandard assumption is the neglection of the advection of momentum in the Navier-Stokes equations, which is justified for the present coarse resolution simulations. When the stratification becomes unstable, convective adjustment is applied. The model is formulated fully implicitly, thus allowing a relatively large time step.

The original code (by Maier-Reimer et al., 1993) has been modified to include vertical diffusion for temperature and salinity. The diffusion coefficient decreases with depth, starting from a value of 0.5 cm^2/s at the surface. The diffusion coefficient is reduced in locations of very stable stratification. The sea ice model has been modified to allow not only transport due to advection by the surface currents of the model, but also a winddriven transport. The ice velocity was set to 3% of the wind velocity, with an geostrophic angle of 23°. Martinson and Wamser (1990) got a good approximation of the ice drift in the Weddell Sea using this relationship.

The atmospheric component consists of an 2-D (longitude-latitude) nonlinear energy balance model comparable to the model of North et al. (1983). The model atmosphere is dry and the only prognostic quantity is the air temperature T. The equation solved for the air temperature is

$$\partial T/\partial t + U\ \partial T/\partial x + V\ \partial T/\partial y + Ah\ \Delta T = (Fsw - Flw + \kappa\ (SST - T))\ /\ (Cp\ \rho\ H),$$

where U and V are the observed zonal and meridional components of the near surface winds, Ah is the horizontal diffusion coefficient ($2 \times 10^6\ m^2 s^{-1}$). The coupling coefficent for heat transfer between surface and atmosphere (κ) is 40 $Wm^{-2}K^{-1}$ over ice free ocean points and infinite over landpoints, corresponding to the assumed zero-heat capacity of landpoints. In icecovered ocean-points, the atmosphere ocean-heat exchange is reduced. The conductive heat flux through sea ice is inversely proportional to the ice thickness and proportional to the difference between the air temperature and the sea surface

temperature (SST) at air temperatures below freezing point. For shortwave and longwave radiation, a constant cloud cover of 40% is assumed. The horizontal distribution of the surface albedos was taken to be the same as in the 'ECHAM3'-AGCM (Roeckner et al., 1992). If the temperature on land points falls below freezing-point, snow cover is assumed. With decreasing temperature, the albedo increases smoothly to 0.85. The albedo for thick sea ice is set to 0.65 (except when it is melting). The long-wave radiation is assumed to be proportional to T_{surf}^4, where the Stefan-Boltzman-constant is multiplied by 0.685 to take the natural greenhouse effect into account and to produce a reasonably realistic distribution of the surface temperature T_{surf}. In the thermal part of the model, no additional flux correction is used.

The atmosphere model runs with a time step of 6 hours. As the atmosphere model is dry, precipitation minus evaporation is required as additional forcing field. A simple river runoff model with a bucket depth of 30 cm is included in the ocean model. It transports the net precipitation over land areas to the ocean. Every day heat and fresh water fluxes are transferred to the ocean surface layer and the runoff model, the change in SST, sea ice thickness and sea surface salinity (SSS) is computed and the first two are transferred back to the atmosphere model. Every 15 days the dynamical part of the ocean model is computed.

The model is forced with monthly climatological surface wind fields, derived from ECMWF-analyses (European Centre for Medium Range Weather Forecasts) from the years 1979-1993. Windstress fields were taken from the monthly climatology of Hellerman and Rosenstein (1983). The monthly climatological fields of precipitation minus evaporation were taken from a 10-year integration with the 'ECHAM3'-AGCM in a T42 resolution forced with observed SST and sea ice distribution (first experiment of the runs discussed by Bengtsson et al. 1996).

In the first phase of the spinup, the surface salinities of the model were additionally restored (with a time constant of 100 d) to the climatological sea surface salinities (SSS) of Levitus (1982). After the model had reached a steady state (after 5000 years of integration), the freshwater fluxes produced by the restoring term were analyzed and added to the prescribed freshwater flux. The additional restoring to climatological SSS was switched off at this stage. The model was integrated with a pure flux boundary condition for freshwater, until after 5000 years of integration a new steady state was achieved, which showed only small differences to the one obtained under restoring conditions for salinity. From this final state, all meltwater experiments were started.

Table 1
description of experiments discussed in the text (except for the initial spinup)

name	meltwater input	wind stress feedback	duration [years]	start	remarks
CTRL	no	no	5000	end of restoring run	used to define climate for feedback model run to steady state
LWF	Labrador Sea	yes	1500	end of CTRL	mostly discussed meltwater experiment
LCW	Labrador Sea	no, climatol. wind stress	1500	end of CTRL	
MWF	Missis. sippi	yes	1500	end of CTRL	

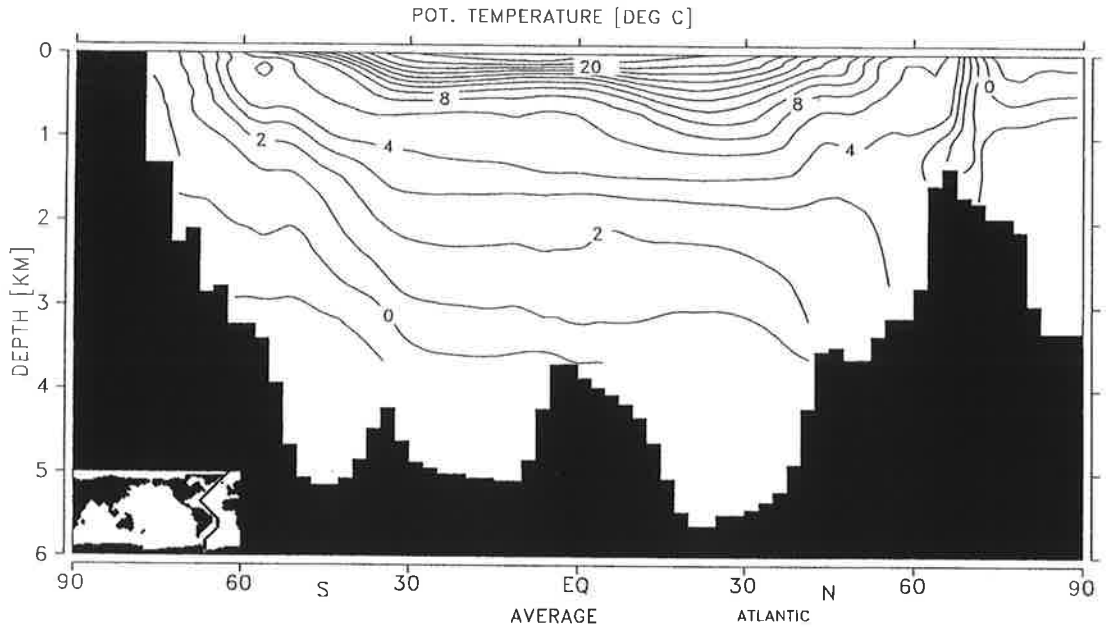

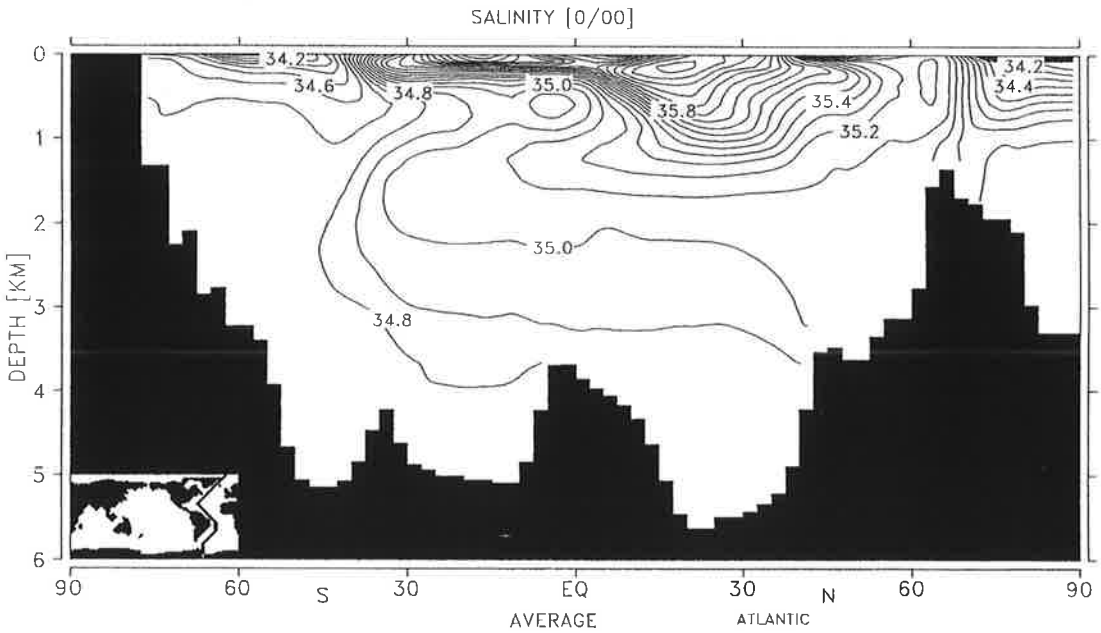

Fig. 1
Meridonal section through the West Atlantic of annual mean potential temperature (a) and salinity (b) of the steady state at the end of the spinup experiment CTRL. The location of the section is shown in the small map.

All experiments were run with seasonal cycle, but in this paper only annual mean data are plotted. A list of the experiments discussed in the text is given in Table 1.

As examples for the ability of the model to reproduce the observed mass distribution in the ocean, sections of potential temperature and salinity through the western Atlantic are shown in Fig. 1. In the deep ocean, temperatures are slightly too cold (between 0.5 and 1°C). The salinity in the deep ocean is slightly too high (error <0.1 psu) almost throughout the deep Atlantic. The position of the fresh tongue of Antarctic intermediate water (AAIW) is correct, but the tongue itself is not fresh enough. The effect of the outflow from the Mediterranean is clearly visible, but seems to be slightly overestimated as deduced from the salinity field. Generally, the model predicts the transition zone between North Atlantic deep water (NADW) and Antarctic bottom water (AABW) at too shallow depths. The depth of the base of the thermocline (e.g. the 6°C isotherm) appears to be reasonably well simulated by this model.

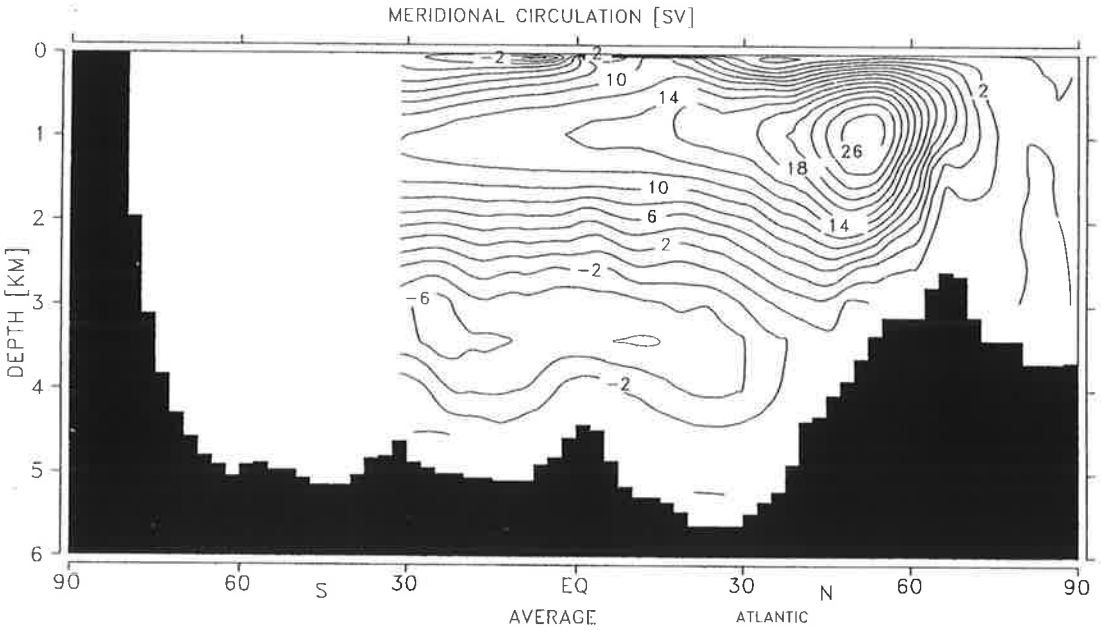

Fig. 2
Meridional overturning stream function of the Atlantic and the end of the spinup (CTRL). Contour Interval is 2 Sv, positive values indicate clockwise rotation.

The zonally averaged mass transport stream function of the Atlantic is shown in Fig. 2. The maximum of the overturning cell in the North Atlantic is 27 Sv. A significant fraction of the NADW is formed in the GIN Sea (Greenland, Iceland and Norwegian Sea). The outflow of NADW into the Southern Ocean is 12 Sv. At the bottom, a deep inflow of 6 Sv AABW can be seen. In the zonal mean, the separation between the NADW cell and the AABW is located at a depth of 2500 m, probably somewhat too shallow compared to the real ocean. It is generally consistent with the picture of the 'conveyor belt' as described in Broecker (1991). The outflow of NADW to the Southern Ocean is about 10% weaker than the current best estimate given by Schmitz (1995).

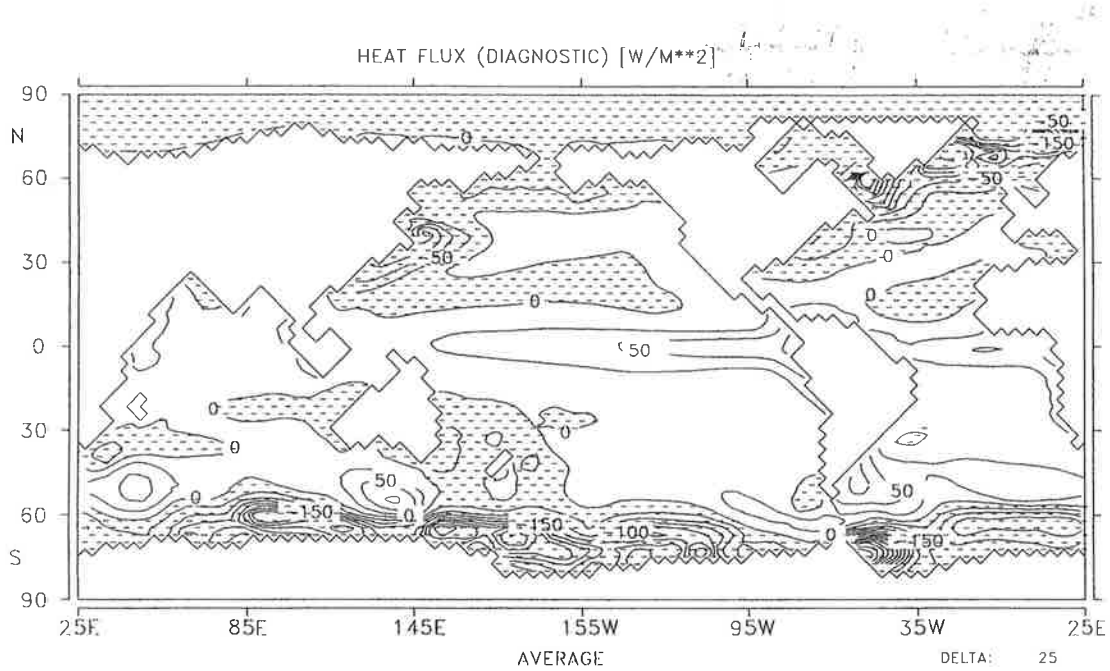

Fig. 3
Annual mean net heat uptake of the ocean in experiment CTRL. Contour interval is 25 $Wm^{-2}K^{-1}$, shaded areas indicate heat loss of the ocean.

In Fig. 3, the net heat flux at the top of the ocean (including sea ice) is shown. In the upwelling regions at the equator the ocean typically takes up 50 Wm^{-2}. Maxima of oceanic heat loss can be seen in the regions of the western boundary currents and in regions of strong deep water formation by convection (Labrador Sea, GIN Sea, Weddell and Ross Sea). The northward oceanic heat transport in the Atlantic at 30°N is 0.88 PW (not shown), in the Pacific it amounts to 0.23 PW. The southward oceanic heat transport at 30°S is 1.1 PW. The heat transport of the North Atlantic is northward at all latitudes with a crossequatorial transport of 0.7 PW. The total oceanic crossequatorial transport is 0.3 PW.

The pure prescription of a climatological wind stress field might be justified for small changes in SST, but large signals in SST as those from meltwater experiments can cause strong changes in the wind stress fields. In meltwater experiments with a fully coupled OAGCM Schiller et al. (1996) have shown that the change in windstress forcing provides an important feedback stabilizing the present mode of the thermohaline overturning. To account for this feedback process, a simple linear statistic feedback model has been included to add a dynamic component to the otherwise thermodynamic atmosphere model.

This statistical feedback model is based on a number of available experiments with the ECHAM3/LSG coupled OAGCM (in addition to a 250 year control run, the experiments included both greenhouse experiments described in Voss et al. 1996 and experiments with collapsed conveyor described in Schiller et al. 1996). From these simulations, monthly mean anomaly fields (relative to the climatological annual cycle of a control run) of near surface air temperature and wind stress were computed after interpolation onto the grid of the present model. Empirical orthogonal functions (EOFs, Preisendorfer, 1988) were computed from the air temperature anomaly fields. The resulting principal component time series were used to construct a linear regression model for the wind stress anomalies. During the simulations, the actual air temperature anomaly field relative to a climatological seasonal cycle is computed. After projection of the field onto the EOFs, multiplication of the resulting principal component coefficients with the regression matrix gives the

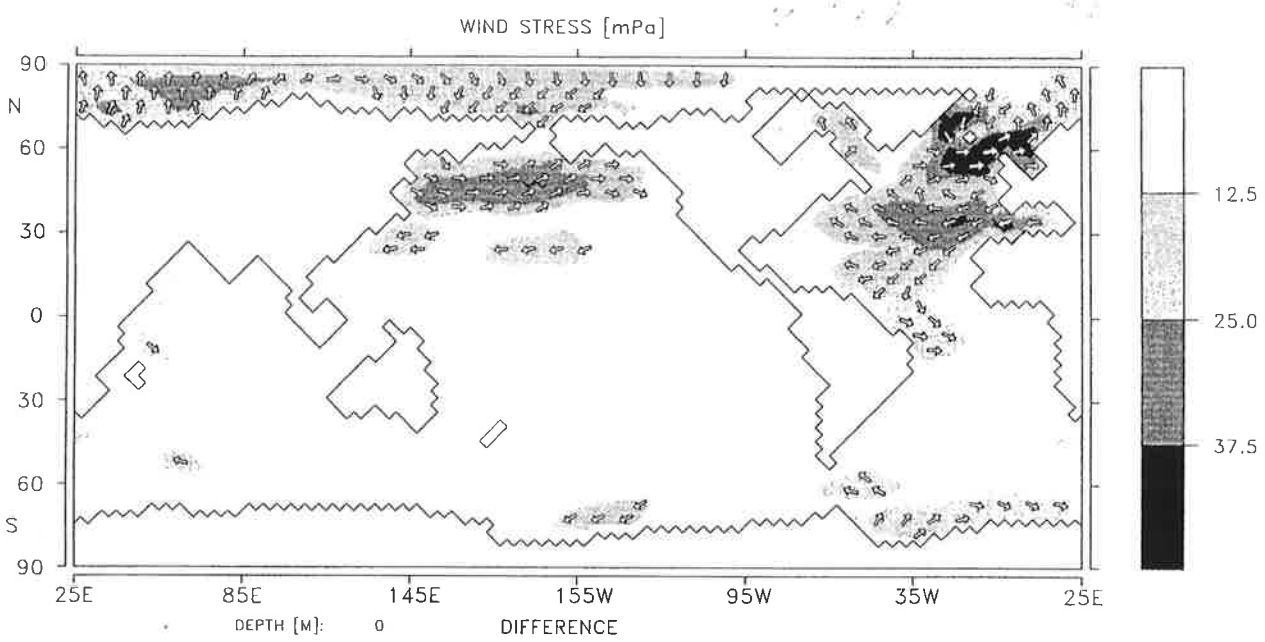

Fig. 4
Mean windstress anomaly derived from the linear regression model for years 326 to 350 of run LWF as compared to the spinup CTRL. The corresponding surface temperature anomaly is shown in Fig. 7. Arrows indicate the direction, colours give are used to distinguish the magnitude of the anomaly. No arrows are plotted for anomalies smaller than 12.5 mPa.

associated changes in wind stress. This type of approach can only be expected to give reasonable results, for temperature anomaly fields which are similar to those occurring in the data used to construct the regression matrix.

In the integrations described in the next section, the air temperature response in the meltwater experiments was essentially contained in the first 2 EOFs of the regression model. Nevertheless, 20 EOFs were used in the standard version of the feedback model to allow for more degrees of freedom in the atmospheric response. The dominant pattern of the resulting windstress anomaly field in case of a collapsed thermohaline circulation and the associated cooling in the northern North Atlantic due to the reduced northward oceanic heat transport is - as in Schiller et al. (1996) - a cyclonic circulation over the GIN Sea (Fig. 4). This leads to enhanced upwelling and to an intensification of the export of fresh surface waters to the North Atlantic by the East Greenland current. Other dominant features are an intensification of the northern hemisphere trade winds in the Atlantic sector and an intensification of the westerlies over the North Pacific.

3. Meltwater experiments

In the present paper the same scenario for meltwater input as in Schiller et al. (1996) was used to facilitate comparison with their experiments with a coupled OAGCM. A meltwater input was prescribed in the Labrador Sea to represent runoff from the Laurentide ice sheet. The amplitude increased linearly for 250 years to a peak value of 0.625 Sv and decreased again to 0 during the next 250 years. The total amount of meltwater added to the system corresponds to an increase of the global mean sea level by 13.4 m. These arbitrarily chosen values are roughly consistent with geological data: Fairbanks (1989) derived global a mean peak value for the last deglaciation of

about 0.45 Sv. This value, however, corresponds to an average over several hundred years. After the meltwater input had reached 0 again in year 500, the model was integrated for another 1000 years without any perturbation in the forcing. The dynamic response of the coupled model is shown in Fig. 5 for a few integral quantities which characterize the large-scale circulation response, for experiments both with and without wind stress feeedback. These two runs will be referred to as experiments LWF and LCW (input into Labrador Sea including wind stress feedback and with climatological wind stress, respectively). Run LWF with wind stress feedback will be discussed as the standard experiment throughout the rest of the paper. The strong prescribed meltwater input caused a rapid cessation of the formation of NADW. Whereas in experiment LCW the system ended up in a stable steady state without NADW, the windstress feedback in run LWF had the effect of strongly reducing the stability of the water column in the GIN Sea and thus did not allow a total suppression of convection. At least intermittent shallow convection is taking place all the time in run LWF, whereas it is totally suppressed in the GIN Sea in run LCW. The outflow of dense water from the GIN Sea to the northern North Atlantic is weakening (see Fig. 6) and the minimum of the overturning streamfunction at 60°N is moving upwards, indicating a shallowing of the outflow. Around year 250 of run LWF, the deep circulation reverses and reaches a maximum around year 400 with a weak northward flow of about 0.7 Sv. After the meltwater supply is stopped, the convection intensifies and deepens continuously. The resulting outflow of intermediate water is also intensifying and deepening. It starts from an intermediate water outflow of 2 Sv between 300 and 900 m. The rate of change intensifies through time. After going through a regime of strong limit cycle oscillations between years 1100 and 1200 (Fig. 5b,d) formation of NADW resumes and the system settles in a circulation pattern similar to the initial state. This shows up as a very rapid change in the meridional overturning until the system settles into an almost steady overturning pattern in the northern North Atlantic (cf. Fig. 6). It should be mentioned that the integration time of this experiment is too short for the ocean to achieve a steady state tracer distribution at the end of any of the meltwater experiments. Therefore there is still a considerable drift in the properties of the deep waters outside the North Atlantic.

Whereas the behaviour of one component of the heat release of the North Atlantic north of 30°N is closely connected to the convection (see Fig. 5d), another fraction with longer time constants is dominated by the flushing of the deep Atlantic leading to a by one to two centuries delayed response of the Atlantic heat transport to the collapse of NADW formation. The formation of AABW is inversely correlated with the formation of NADW, with a similar delay. AABW formation reaches a maximum around year 300 and then slowly decays for the rest of experiment LWF.

In a third meltwater experiment, the location of the meltwater input was changed. Now the meltwater was released into the Mississippi, following the other potential path for the meltwater from the Laurentide ice sheet. Amount and temporal evolution of the prescribed meltwater input correspond to the experiments with meltwater input into the Labrador Sea. This experiment was run with windstress feedback. It will be referred to as run MWF (input into Mississippi, with wind stress feedback). For the first few hundred years, experiment MWF shows a marked delay in the response compared to the Labrador experiment LWF. This can be explained by the difference in advection time scales to the locations of deep convection in the North Atlantic and by the dilution of the signal during its advective propagation to the northern North Atlantic. After the formation of NADW has stopped, both curves converge and show - except for a delay of approximately three decades in run MWF - an almost identical response for the second half of the experiment. Since the location of the input has a strong effect on the threshold value for a collapse of the 'conveyor-belt'-type thermohaline circulation (with

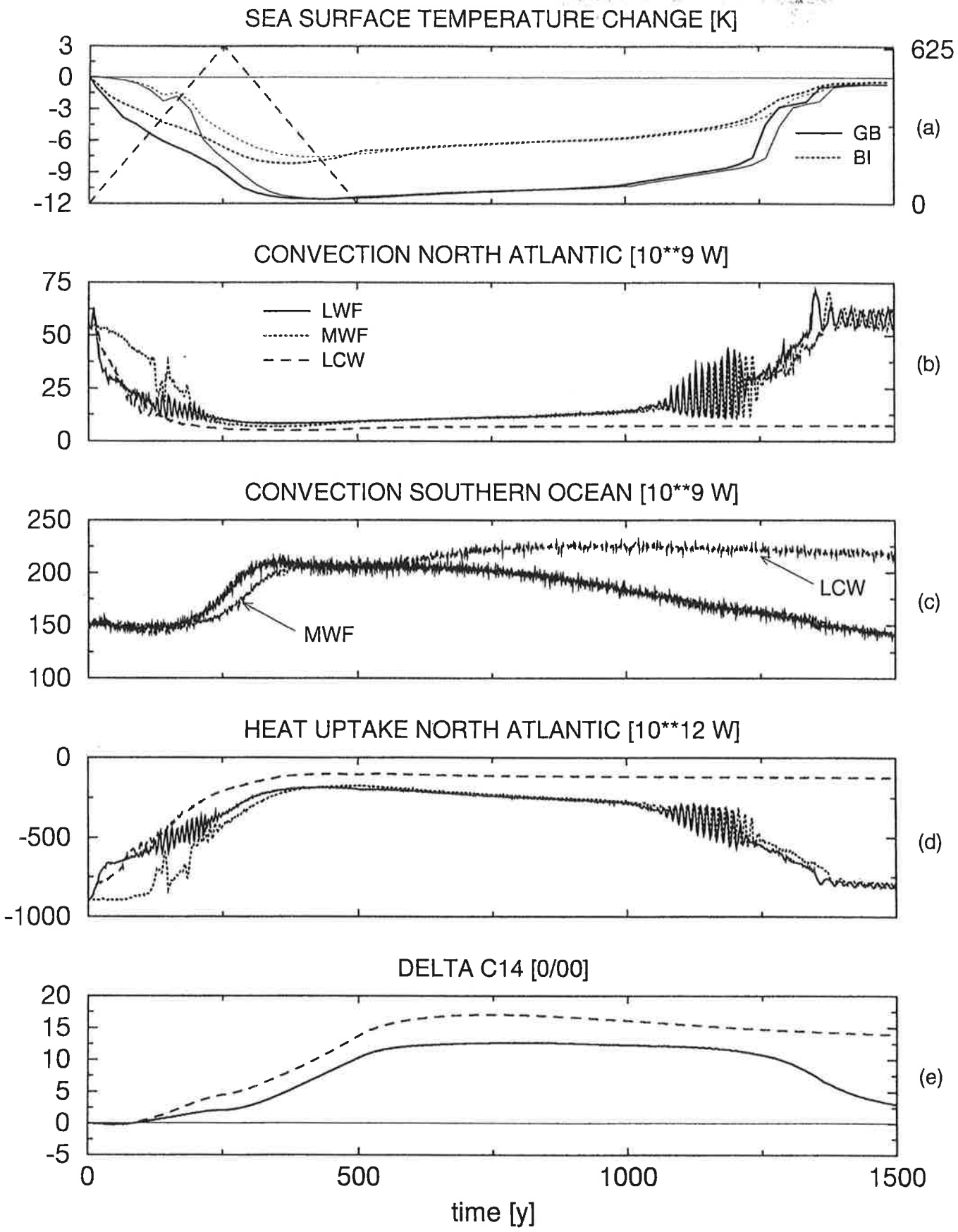
SEA SURFACE TEMPERATURE CHANGE [K]
3
0
-3
-6
-9
-12
625
0
GB
BI
(a)
CONVECTION NORTH ATLANTIC [10**9 W]
75
50
25
0
LWF
MWF
LCW
(b)
CONVECTION SOUTHERN OCEAN [10**9 W]
250
200
150
100
LCW
MWF
(c)
HEAT UPTAKE NORTH ATLANTIC [10**12 W]
0
-500
-1000
(d)
DELTA C14 [0/00]
20
15
10
5
0
-5
0
500
1000
1500
time [y]
(e)

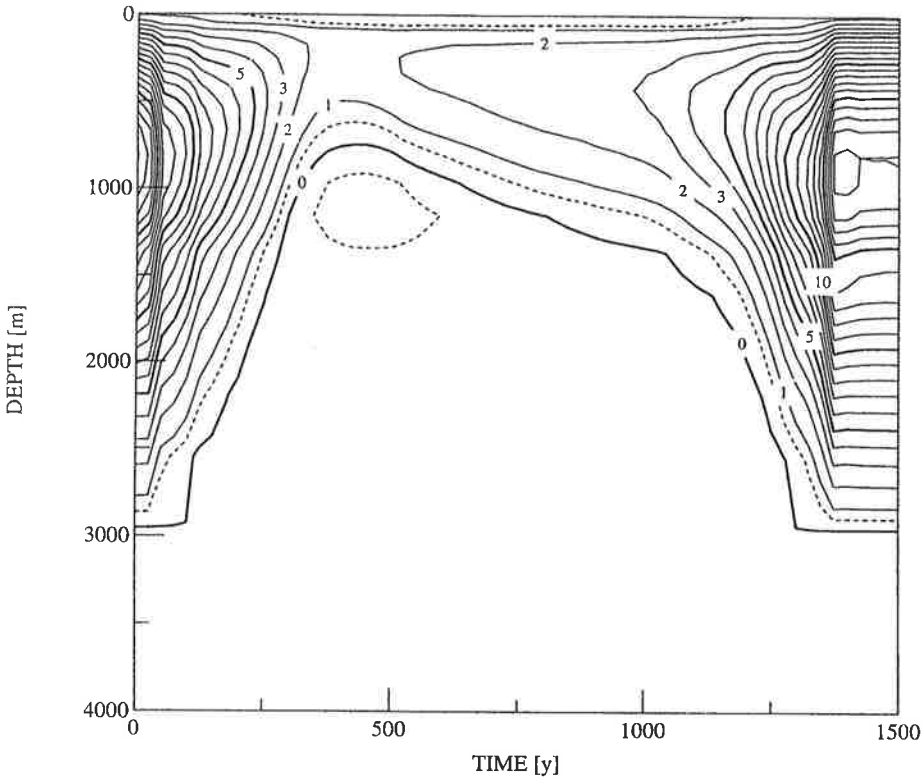

Fig. 6
Hovmøller plot of the Atlantic meridional overturning streamfunction at 60°N of the standard meltwater experiment LWF. Positive values indicate surface inflow and deep outflow. Data are computed from 25-year averages of the data. Contour Interval is 1 Sv, additional dashed lines are shown for +/-0.5 Sv.

Fig. 5 (opposite page)
Time series plots of the meltwater experiments. Panel (a) shows time series of 25 year averages of SST anomalies at two locations in the northeast Atlantic at 16°W and 54°N (GB), and at 11°W and 44°N (BI), respectively. Results shown for experiments LWF (thick line) and MWF (thin line). The triangular shape dashed line shows the prescribed meltwater input. For this curve the scale on the righthand side is applicable. All other time series in this Figure indicate annual mean values without additional filtering. In all other panels experiment LWF is represented by the solid line, run LCW by a dotted line and run MWF by the dashed line. Panel (b) shows the time evolution of the release of potential energy by convection in the North Atlantic (a proxy of the formation rate of NADW). Panel (c) is a display of the same quantity as (b) for the Southern Ocean, now a proxy for the formation rate of AABW. The next panel (d) shows the heat uptake of the North Atlantic (all ocean grid points in the Atlantic and Arctic north of 30°N. Negative values indicate heat loss of the ocean. The last panel (e) shows the resulting atmospheric Δ14C values.

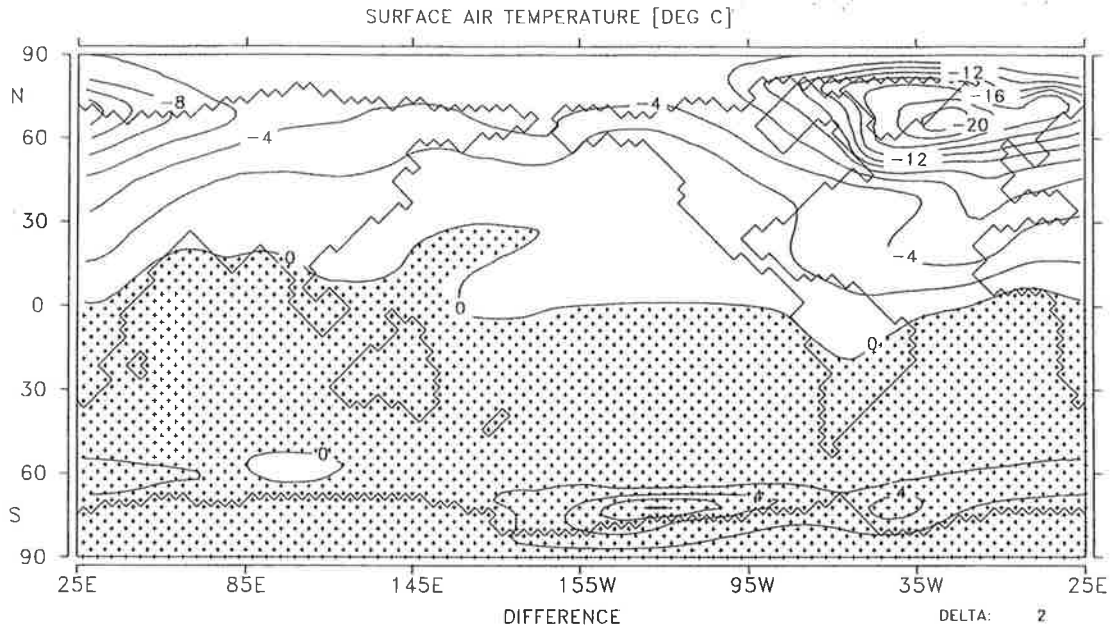

Fig. 7
Annual mean difference in surface air temperature averaged over years 326 to 350 of run LWF relative to the climate at the end of the spinup CTRL. Contour interval is 2°C, shading indicates positive values.

significantly higher threshold values for the Mississippi case), as proposed by Broecker et al. (1989) and confirmed in the OGCM-only experiments by Maier-Reimer and Mikolajewicz (1989), the prescribed meltwater input must be well above the threshold values for both input locations.

The changes in oceanic heat transport (mainly in the Atlantic) are also associated with strong changes of the temperature distribution. As an example, the changes in annual mean surface air temperature (averaged over years 326 to 350 of experiment LWF) compared to the initial steady state are shown in Fig. 7. The most obvious pattern is the strong cooling over the northern north Atlantic and the GIN Sea with extreme values in the annual mean of more than 20°C. It is related to a southward movement of the sea ice margin (not shown). The cooling over sea ice is even more pronounced in the northern hemisphere winter. In the SST fields, the area of strongest cooling is shifted towards the southeast with a maximum of more than 10°C west of Scotland (not shown). The cooling extends over most of the northern hemisphere. In the southern hemisphere there is a weak tendency towards warmer temperatures. The maxima in the Pacific sector of the Southern Ocean are associated with an intensification of the convective activity and a corresponding retreat of the sea ice margin. All effects and their magnitude are well in agreement with the results of the integration with the coupled OAGCM of Schiller et al. (1996).

The temporal evolution of the SST anomaly is shown for two locations in Fig. 5a. In both experiments, the temperature response clearly lags the prescribed meltwater input, the lag being larger in case of a Mississippi input.

4. The response in tracers

4.1 Implications for radiocarbon

In the model, Δ14C is treated essentially like Toggweiler et al. (1989) did in the GFDL model. Because of the free surface of the LSG model and associated changes in the volume of the uppermost grid boxes through the net freshwater fluxes, Δ14C had to be formally split up into two tracers for the sake of mass conservation. Thus Δ14C in the model is diagnosed as the ratio between two tracers, 14C and an additional tracer. This tracer differs from 14C only in the lacking source in the atmosphere and the missing radioactive decay.

During the spinup, the atmospheric Δ14C was held constant at a standard value. This value serves also as atmospheric standard for later integrations. Radiocarbon is treated in the model as a passive tracer, transported like active tracers (e.g. salinity) by advection, convection and diffusion. At the surface the concentrations are subject to exchange with the atmosphere, the globally averaged piston velocity being 9 m/y. Locally the piston velocity varies proportionally to the gas exchange coefficient calculated by the formula given by Liss and Merlivat (1986). The atmosphere has a reservoir size corresponding to 80 m of water. The radiocarbon field is additionally changed by radioactive decay. The transport of radiocarbon from the surface to the interior of the ocean by sinking biogenic particles is ignored. In the meltwater experiments the production rate of 14C was kept constant at a value required to keep the atmospheric concentration at a constant level in the spinup run CTRL. The resulting distribution of Δ14C along a meridional section through the western Atlantic is shown in Fig. 8. The plot clearly reveals the characteristic patterns of the distribution of Δ14C in the Atlantic. Due to the exchange with the atmospherethe water at the surface is relatively young. In the North Atlantic, a well mixed zone reaching to the bottom can be seen in the area of deep convection. The relatively young water flows southward in the deep western boundary current at a depth of around 1500 m. In the deep Southern Ocean, the model produces water masses with values below -130 ‰. This is slightly younger than the observed values (up to -160 ‰ in the West Atlantic GEOSECS section, Stuiver and Östlund 1980). The model clearly shows the tongues of old water in AAIW and AABW, but generally the signals in these tongues are not as marked as they show up in observations.

With the assumption that radioactive decay is the only process causing deviations from the atmospheric standard ratio, all Δ14C values of the ocean can be transferred into an apparent radiocarbon age relative to this standard. This age gives an estimate of the average time elapsed since the water particle has last been in equilibrium with the atmosphere. However, due to the permanent mixing with underlying older water and the long time constant for the equilibration process at the surface, complete equilibrium with the atmosphere will never be reached in the ocean. The radiocarbon age distribution at the surface of the ocean is shown in Fig. 9. In the nonpolar Atlantic, typical reservoir ages vary between 270 and 500 years and are not too different from the standard value of 400 widely used in the 14C-dating of marine sediment cores. In areas of strong deepwater supply (both in the upwelling zone of the tropical Pacific and the areas of deep convection), the ages become significantly higher. The high ages below sea ice in the model are strongly dependent on how the gas exchange in the presence of sea ice is treated. In this model, it is assumed that the piston velocity approaches 0 as the sea ice grows thicker than 10 cm.

As a result of the changes in the ventilation of the deep ocean in the meltwater experiments, the atmospheric 14C/12C ratio changes as well (see Fig. A05e). The collapse of the NADW formation causes the atmospheric Δ14C value to rise as the effectively ventilated ocean volume becomes smaller. The increase

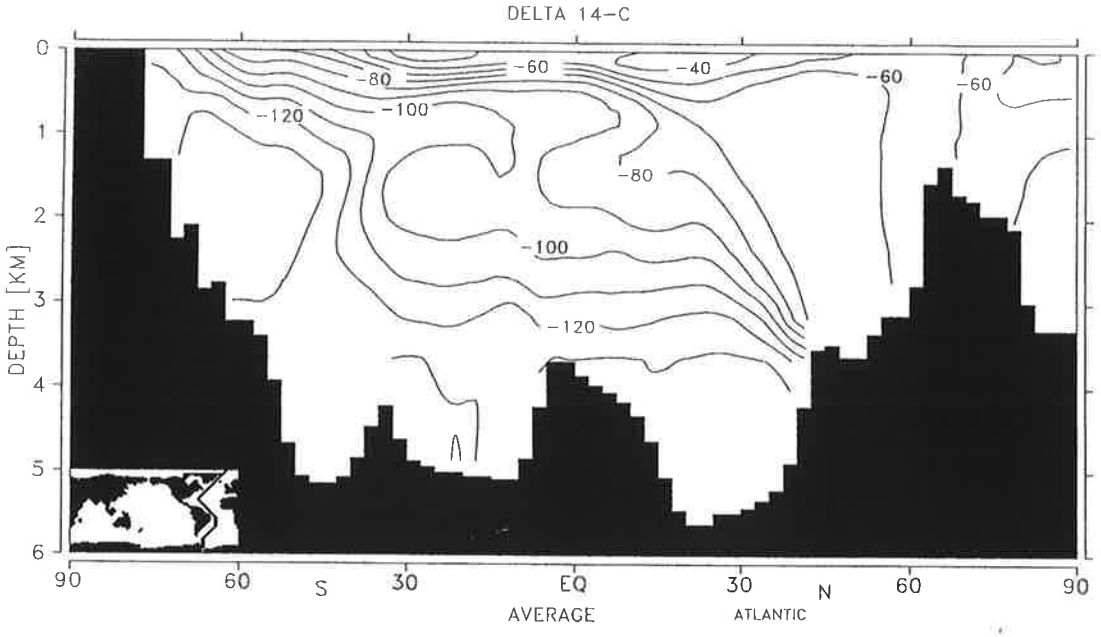

Fig. 8
Climatological Δ14C at the end of the spinup CTRL on a merdional cross section through the West Atlantic. The location of the section is shown in the small map. Contour interval is 10‰.

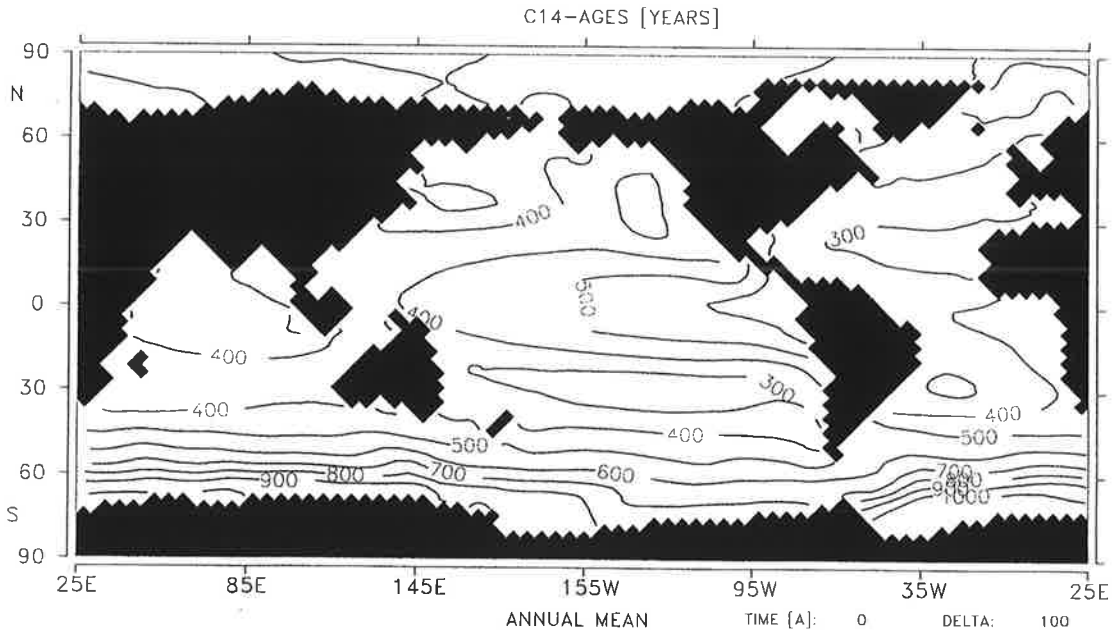

Fig. 9
Radiocarbon age (in years) in the first layer of the ocean at the end of the spinup CTRL.

is strongest around year 400 while it levels off at year 500. A maximum value of 13 ‰ is reached in year 600. In the following years, the atmospheric Δ14C slowly decreases again. The onset of strong NADW formation in year 1300 amplifies the decrease of atmospheric concentrations. At the end of the experiment in year 1500, the atmospheric concentration is still 5 ‰ above the value of the initial state with decreasing tendency. In this model, the terrestrial biosphere is not included. Due to the increase in reservoir size, the net effect of the terrestrial biosphere should be a damping of the variations in atmospheric Δ14C.

In many geological records the dating (at least down to the last glacial maximum) is commonly performed by computing radiocarbon ages from measured Δ14C values. Thus, radiocarbon is widely treated as a 'clock' indicating the age of a sample. This is simulated in the present model by using the actual Δ14C values of the model, transferring them into radiocarbon ages and adding the actual value of the model clock. The relation between the radiocarbon 'clock' calculated from ocean surface data of run LWF and the real time evolution (that is the model clock) is shown in Fig. 10a for a number of typical North Atlantic locations together with the 'clock' derived from the atmospheric radiocarbon. If the radiocarbon 'clock' would be an ideal indicator of the true age of a sample, the relation would be a straight line with the slope 1. To account for the typical radiocarbon ages at the surface of the ocean, a constant reservoir age of 400 years was subtracted from the atmospheric values to allow better comparison to individual radiocarbon 'clocks' at different locations. Similar corrections have been made in many paleoceanographic studies. When NADW formation is suppressed, all curves show that the radiocarbon 'clock' is too fast due to the increase of the atmospheric Δ14C values. When the conveyor belt circulation resumes, the curves indicate almost a standstill of the radiocarbon 'clock'. The deviation between the individual chronologies constructed from different locations is of the order of 100 years. Changes in the surface concentrations of Δ14C are caused by changes in the residence time at the surface and in the rate of mixing of deeper waters with a higher degree of depletion in radiocarbon. The deviations between the chronologies at different locations are largest during times of rapid circulation changes. During the first few hundred years, there is a general tendency towards an advancing radiocarbon 'clock' as the stability of the water column increases and the residence time at the surface becomes larger. In the global average, this leads to relatively high concentrations of radiocarbon in the atmosphere, the effect being most pronounced in the surface layer of the North Atlantic. In ice-free water, potential changes in the gas exchange coefficient were ignored in this experiment. The inclusion of this effect might have lead to even larger deviations between the apparent radiocarbon chronologies taken from different locations at the same time horizon. The absolute size of the deviations in chronologies from radiocarbon 'clocks' between different locations strongly depends on the magnitude of the prescribed piston velocity, since an increase in the global mean piston velocity has the effect of reducing local differences in the surface distribution of Δ14C.

In the deep ocean the changes in Δ14C distribution are quite large, as can be seen from Fig. 10b. In the beginning of experiment LWF, the time series of the radiocarbon 'clock' at 2357 m off the Caribbean shows a reversal of the deep radiocarbon chronology after the formation of NADW has been suppressed. This can only be explained by advective effects rather than by a pure stagnation and aging of NADW.

The model was run including 'coloured tracers' allowing to trace watermasses immediately back to their origin. The surface concentrations of these tracers were set to 1 in their defined source areas and 0 elsewhere. The most important coloured tracers where those tracing AABW and NADW in the deep ocean

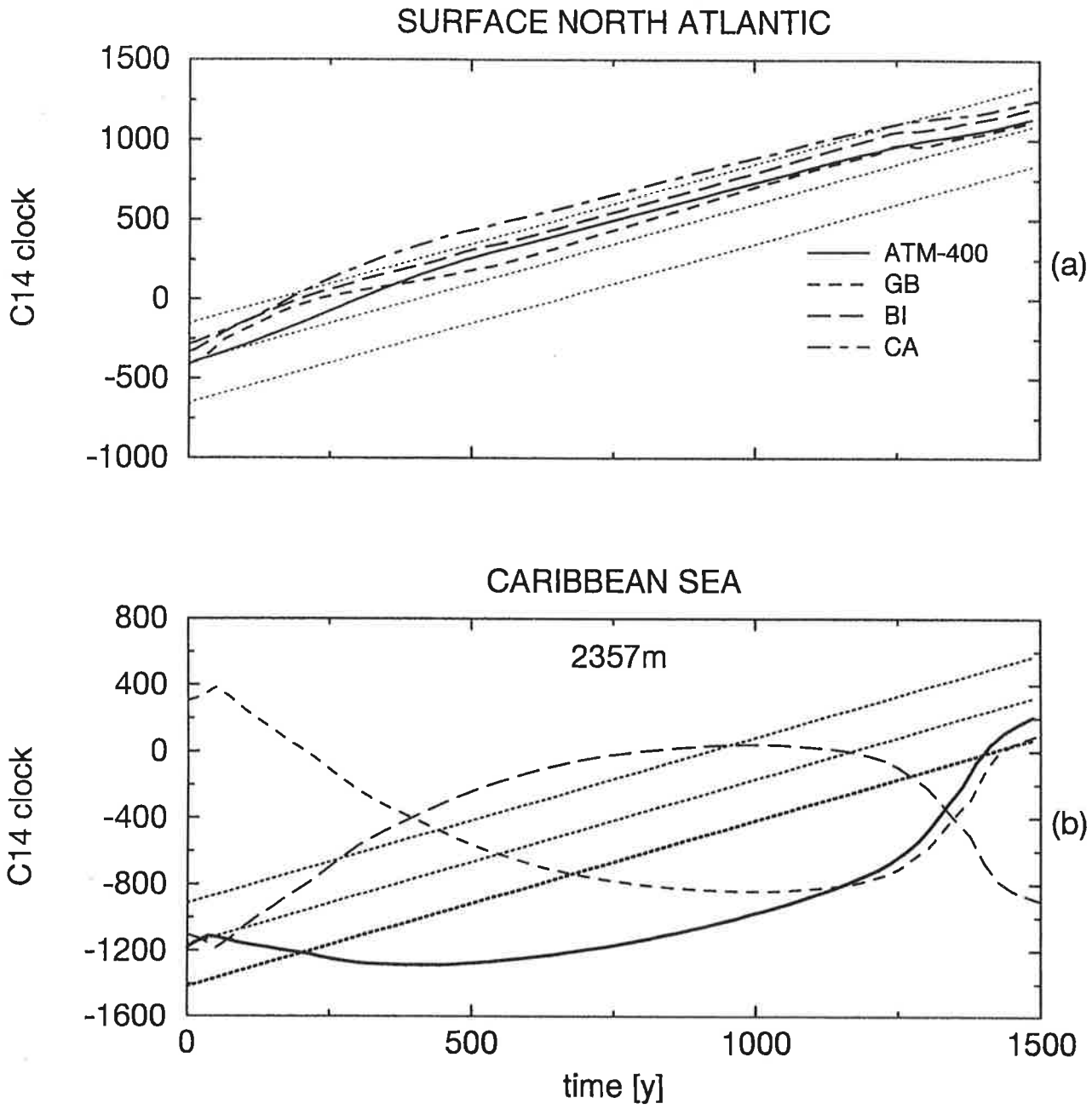

Fig. 10
Radiocarbon 'clock' vs. real time (model clock) derived from data averaged over 25 years in run LWF. The top panel (a) shows the time evolution of radiocarbon 'clock' for the atmosphere (corrected for a reservoir age of 400 years, solid line) at three different locations: two in the northeast Atlantic (GB, BI), one off the Caribbean (CA). The thin dotted lines indicate lines corresponding to radiocarbon clock equals real time plus constant. The dotted lines are drawn 250 years apart from each other. The lower panel (b) shows the evolution of radio carbon 'clock' at 2357 m depth off the Caribbean (solid line). The two dashed curves show the relative contribution of 'coloured tracers' indicating relative contributions of AABW (short dashed) and NADW (long dashed). The respective scale for the 'coloured tracers' is on the right.

with defined source regions in the Southern Ocean south of 30°S and in the Atlantic north of 30°N, including the Arctic, respectively. Time series of the concentrations of the 'coloured tracers' indicating the relative contributions of NADW and AABW to the water mass properties at this location in the deep Caribbean are plotted in Fig. 10b, too. The suppressed supply of NADW causes the boundary between relatively young NADW and relatively old AABW to shift upward, thus leading to an increased contribution of AABW chartacteristics to the watermass properties at this location. This advective effect explains the rapid increase in the radiocarbon age of the deep water. The relative contribution of AABW starts from about 20% and reaches 50% in year 375 of the experiment. The relative contribution of NADW shows the inverse signal, starting from about 80%. After the strong initial signal, the radiocarbon clock is loosing almost 800 years, thus producing increased age differences between surface and deep Atlantic. The relative contribution of AABW increases, until reaching a maximum of 70% around year 1000. Finally, after onset the of strong NADW formation and a sufficient deepening of the associated overturning cell, the advection of young NADW and a corresponding reduction of the relative contribution of AABW lead to a sudden decrease of the radiocarbon age of the deep water compared to the surface and hence the deep radiocarbon 'clock' is rapidly advancing.

The distribution of the differences in radiocarbon ages between the surface layer and the layer centered at 2357 m is shown in Fig. 11 for the control run CTRL and the the average between years 676 to 700 of the meltwater experiment LWF. In this time slice the age differences are close to their maximum. In the control run, the age differences between surface and 2357 m clearly reveal the path of the deep fractions of the southward propagating NADW as a western boundary current. Except for the Southern Ocean, water masses in the western boundary current show an increase in age from north to south. This is consistent with the general flow pattern. Towards the east the water becomes generally older. Off New Foundland, the radiocarbon age difference relative to the surface is considerably below 200 years, whereas at the west coast of Africa the deep waters are generally more than 800 years older than the surface waters. Around Antarctica, age differences are very small. It should be pointed out that around Antarctica the radiocarbon age in the surface waters reaches values of more than 1000 years under sea ice (cf. Fig. 9). The same water transported in deep levels into the low latitude Atlantic would show up as old water due to the changes in the radiocarbon age of the surface waters.

700 years later the water in the North Atlantic has become much older. Around 30°N deep waters have now radiocarbon ages more than 1400 years compared to the age of the respective surface waters. With the exception of the Southern Ocean, the Atlantic is now filled with waters more than 1100 years older than the respective surface waters. As the formation rate of AABW has increased slightly, the water close to the coast of Antarctica still has similar radiocarbon ages as the respective surface waters, but the gradient across the ACC has increased strongly.

4.2 Implications for the distribution of oxygen isotopes

Another geologically important tracer is δ18O. In the interior of the ocean δ18O of sea water is a conservative tracer like salinity. Following Lehman et al. (1993), a constant δ18O value of -17.4 ‰ was assumed for the net freshwater flux at the ocean surface. The fractionation between 16O and 18O occurring during formation and melting of sea ice is small, and is therefore neglected here. For the nonpolar surface ocean, this approach leads to a ratio between differences in salinity and δ18O of 2 psu: 1 ‰. This is fairly coherent with what Craig and Gordon (1965) reported for the real ocean. The relation between δ18O and salinity for the surface layer in the Atlantic

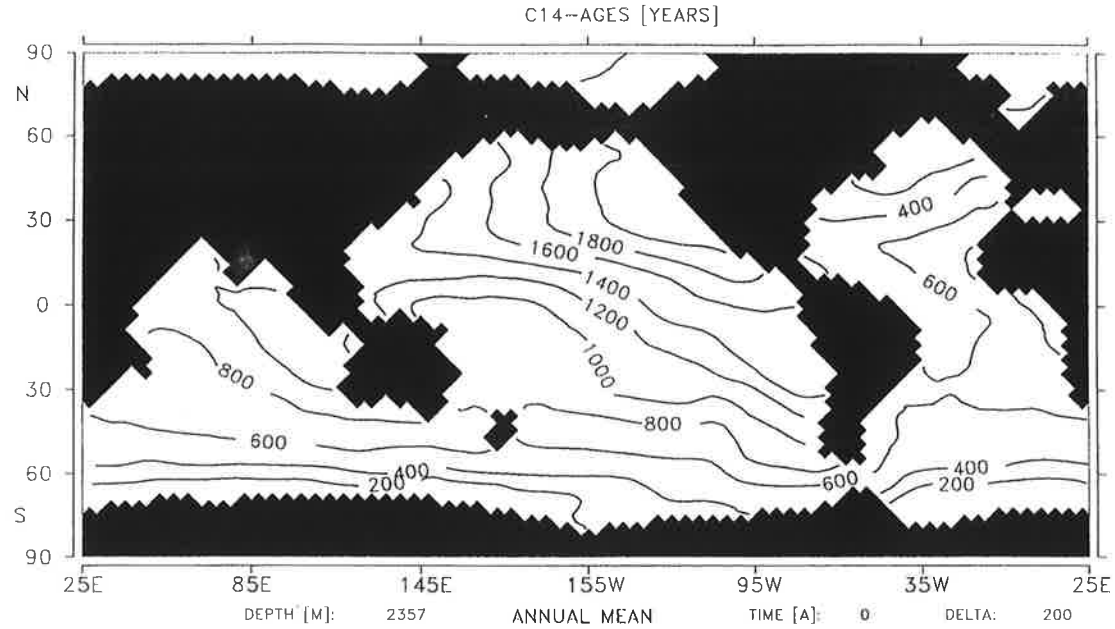

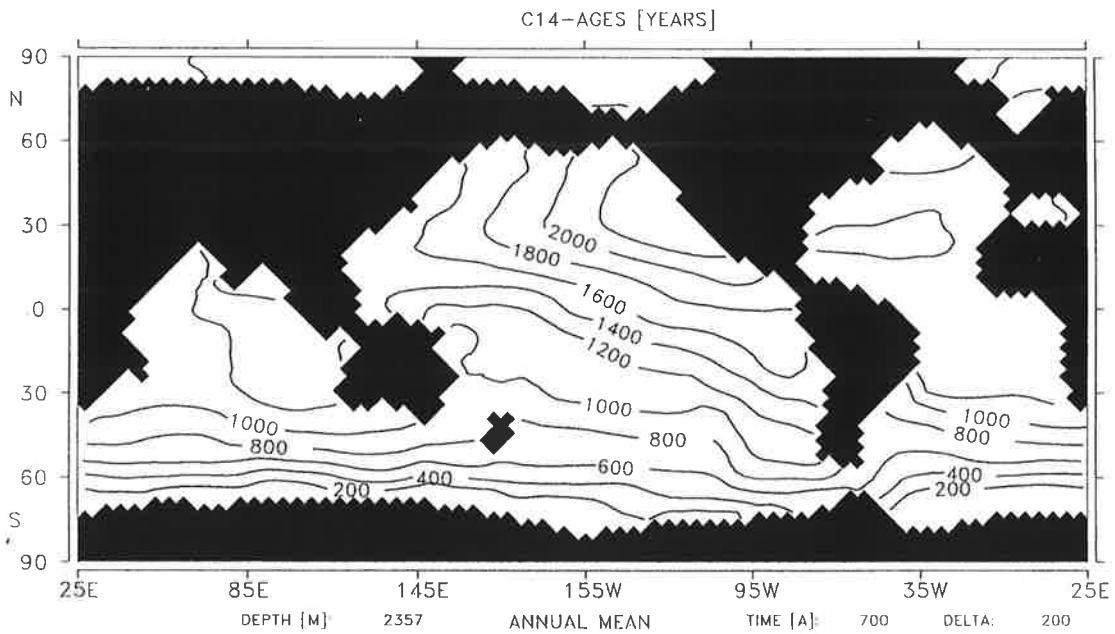

Fig. 11
Difference in radiocarbon ages between deep (2357 m) and surface level for the end of the spinup CTRL (a) and averaged over years 676 to 700 of experiment LWF (b).

(excluding the Arctic, the Hudson Bay and the Labrador Sea, where the sea ice effect is dominating) that results from such an approach is shown in Fig. 12b. Most data points follow directly the relationship between δ18O and salinity that was implied by the δ18O in the net freshwater fluxes. Compared to the implied relationship, δ18O is slightly too high in the surface layer. This can be explained by the effect of mixing with water containing a contribution from melted sea ice. For comparison, Fig. 12a shows the same relation for the GEOSECS data in the top 200 m of the Atlantic. The data roughly follow the relationship assumed in this model, but the scatter around the implied relationship is significant. Similar relationships have been used to reconstruct past salinities from δ18O data from marine sediment cores (e.g. Duplessy et al., 1991; Duplessy et al., 1992; Wang et al., 1995).

In this experiment it was assumed that the added meltwater stemming from the isotopically depleted Laurentide ice sheet has an δ18O value of -40 ‰. It must be stressed, however, that the whole experimental setup provides only a very crude representation of the δ18O cycle in the atmosphere-ocean-cryosphere system and ignores many potentially important processes. In reality, for instance, the δ18O value of the surface fluxes strongly depends on the δ18O values of the precipitation which in turn is strongly affected by the atmospheric circulation. The δ18O of the evaporation is a function of both surface temperatures and the δ18O values of the vapour above the ocean.

In Fig. 13a,b, timeseries of the δ18O in surface seawater in the Bay of Biscay and off the Caribbean from experiment LWF are shown, with a time series of the salinity at these positions. In a qualitative way, δ18O and salinity clearly show a very similar temporal evolution, but a quantitative reconstruction of salinity from δ18O would produce errors of about 1 psu or 20% of the signal, despite the fact that both locations are chosen to be far away from both the sea ice margin and the location of the meltwater input. In areas with active sea ice, the good relationship between δ18O and salinity is strongly disturbed and the errors in the reconstructed salinity become even larger.

Due to the meltwater input with its different δ18O values, the relationship between δ18O of seawater and salinity changes. This is demonstrated by the scatterplot of δ18O vs. salinity at the surface of the Atlantic (Fig. 12c) averaged over years 326 to 350 of run LWF. It is obvious that the previously assumed relationship between these quantities is no longer valid. After the meltwater input has stopped, the relationship slowly starts to reestablish itself (see Fig. 12d), but at a slightly lower δ18O level for the same salinity due to the assumed changes in ice volume.

As an example for the response in the deep ocean, the time evolution of the deep δ18O of sea water is shown off the Caribbean (Fig. 13c). The δ18O values are gradually decreasing by about 0.3‰. Around year 1300, the arrival of new NADW causes a rise of 0.25‰ within less than 200 years. In most locations of the deep Atlantic, the same typical behaviour can be found.

Sediment cores do not preserve the δ18O value of sea water but they preserve the δ18O of carbonate. This quantity is usually assumed to be a function of both the δ18O value in sea water and the temperature relevant for the growth of the shells. In the literature several different equations for the temperature correction are proposed (cf. e.g. Zahn and Mix, 1991). In this paper, the inversion of the paleotemperature equation given by Duplessy et al. (1991) is used

$$\delta 18O_{carb} - \delta 18O = 21.9 - \sqrt{310.61 + 10 \times T}$$

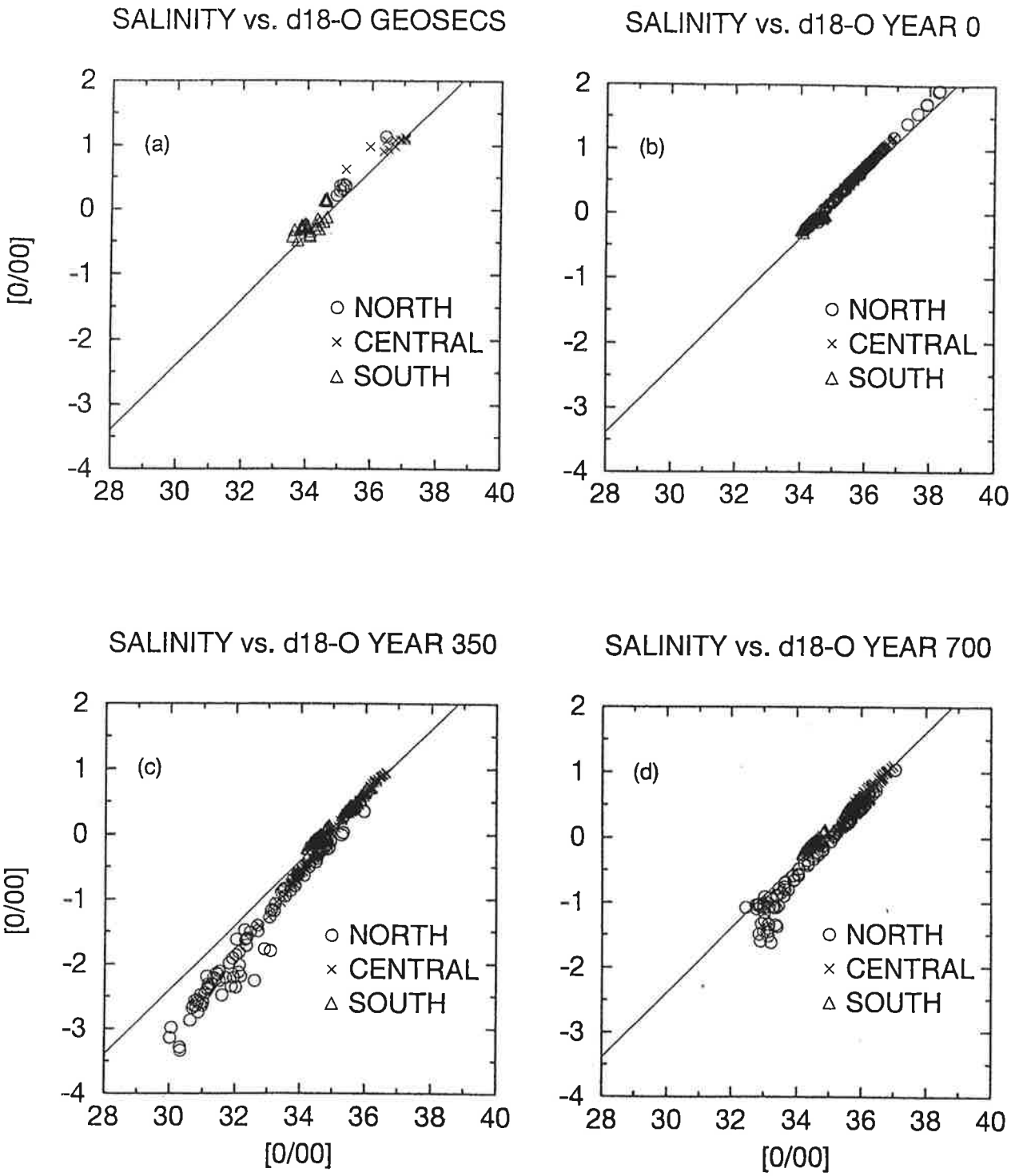

Fig. 12
δ18O vs. salinty in the surface Atlantic (excluding Labrador Sea and Hudson Bay). Model results for the surface layer are shown for the final state of the spinup CTRL (b), as well as for years 326 to 350 (c) and years 676 to 700 (d) of run LWF. Observations from the GEOSECS expeditions (for the upper 200 m) are shown in panel (a). The thin line corresponds to a 2:1 ratio.

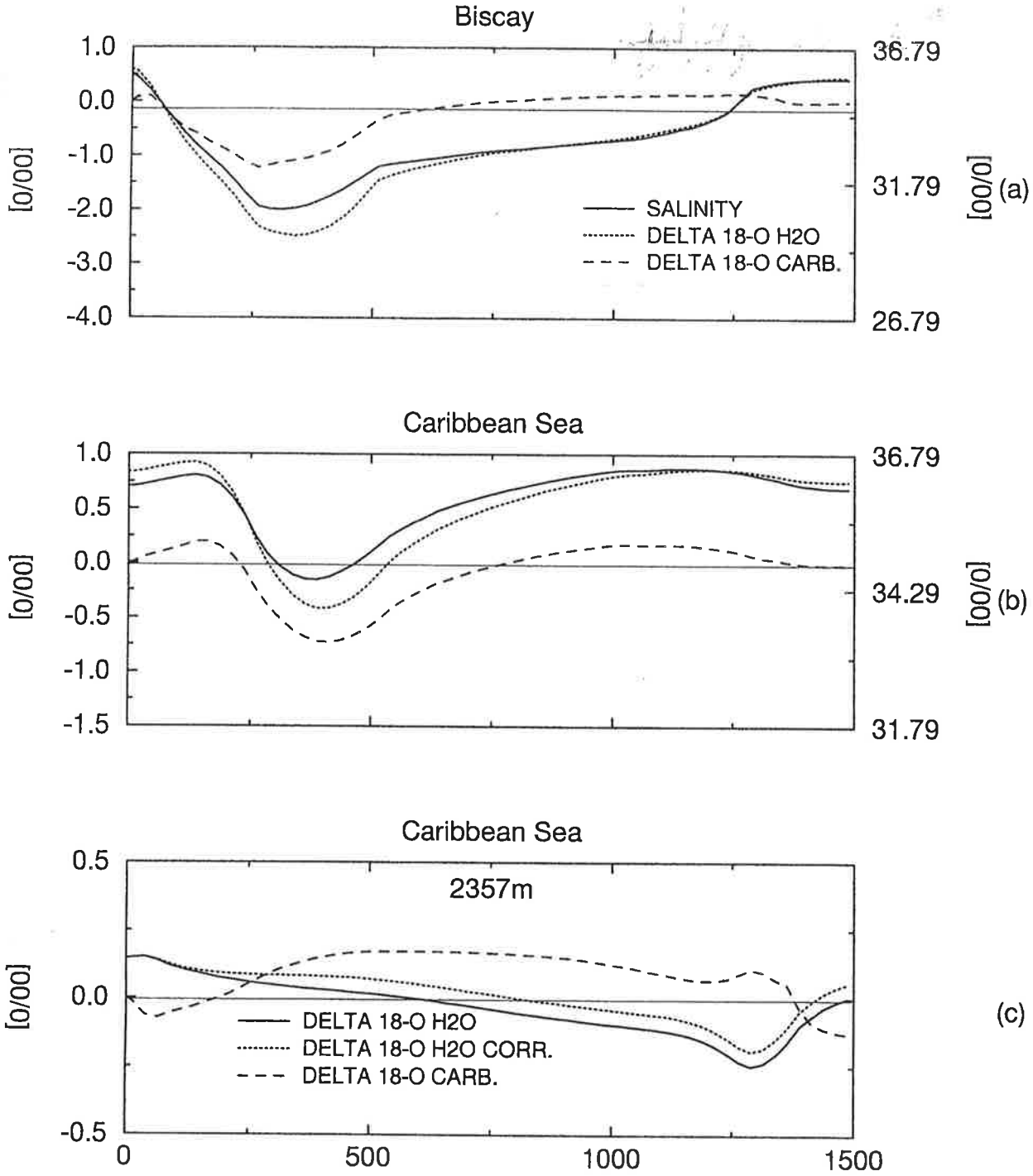

Fig. 13
Time series (derived from data averaged over 25 years) from run LWF. The top two panels show surface data from the northeast Atlantic (a, at 11°W and 44°N) and off the Caribbean (b). The solid line shows the surface salinity, the dotted line is the δ18O of sea water. The scale on the lefthand side refers to δ18O, the scale on the right hand side to salinity. The scales are plotted so as to allow the interpretation of the δ18O as 'reconstructed' salinity, using the implied relation between δ18O and salinity anomalies. The dashed curve shows anomalies of the time series of $\delta 18O_{carb}$ that would be recorded in planktonic carbonate shells (anomalies). In panel (c), the time evolution of δ18O in sea water (solid), the record corrected for the effect of the change of global ice volume (dotted line) and the final resulting record (anomalies) of $\delta 18_{carb}$ (dashed line) are shown at 2357 m depth at a location off the Caribbean.

For the purpose of simplication, the local annual mean temperature T (in $^{\circ}C$) is used in this paper. In Fig. 13, the resulting curve of $\delta 18O_{carb}$ is also shown for both the surface level and the level at 2357 m depth. At the surface, the temperature effect (cooling) cancels most of the direct meltwater effect in $\delta 18O_{carb}$. These two effects can be separated to some extent by the use of plankton abundances.

In the deep Atlantic (see Fig. 13c), the signals in $\delta 18O$ are much smaller. The temperature effect (more than $1^{\circ}C$) on $\delta 18O_{carb}$ through changes from a NADW dominated regime to an AABW dominated regime is larger than the reduction in $\delta 18O$ in sea water. This cancellation of temperature effect and meltwater signal in $\delta 18O$ is a characteristic feature of all locations in the deep North Atlantic which are originally in a NADW dominated regime. In the model, the temperature effect is dominating at most locations. An exact independent estimate of deep ocean temperatures from sediment cores alone seems to be difficult. Therefore, it can be expected that it is to be almost impossible to clearly separate these two effects in $\delta 18O_{carb}$ in real sediment cores on the relevant time scales.

5. Discussion

Although the experiments discussed in this paper are sensitivity experiments with idealized conditions and are not an attempt to reproduce climate variations for any specific period, it is tempting to see whether the characteristic response to meltwater input found in the model has anything in common with signatures found in geological records of the deglaciation. The difficulty is again that the model so far contains only few variables that can directly be compared to records from marine sediment cores.

At least some of the physical effects found in the model simulations can be compared to geological records from the last deglaciation. The most pronounced cooling event in the record was the Younger Dryas. The maxima and the horizontal extent of the cooling signal in surface temperatures as it is reported e.g. in Broecker et al. (1988) with a maximum over Europe and the northern North Atlantic is in qualitative agreement with the temperature changes found in the model. Sowers and Bender (1995) recently reported a sharp cooling signal in Antarctic ice records durimg the Bølling-Allerød warm period and a slight warming during the Younger Dryas cold spell. This inverse correlation was found in the present model, too. The rapid end of the cold event found in the model (cf. curve Fig. 5a) has its correspondence in the abrupt termination of the Younger Dryas signal in Greenland ice cores. Dansgaard et al. (1989) report that the transition to holocene values at the end of the Younger Dryas happened within 20 years.

Boyle and Keigwin (1987) and Keigwin and Lehman (1994) report $\delta 13C$ minima on the Bermuda rise during the Younger Dryas which are likely to occur in case of the upward movement of nutrient rich AABW and the stagnation of NADW. Sarnthein and Thiedemann (1990) report a typical signature of negative $\delta 13C$ peaks and a positive $\delta 18O$ signal in benthic forams during the last six deglaciations. The signal in deep $\delta 18O_{carb}$ is small, as is the case in the model discussed here. Some records show a shoulder or even a small minimum during the rise of deep $\delta 18O_{carb}$ (e.g. Boyle and Keigwin, 1987; Sarnthein and Thiedemann, 1990). In comparison with absolute chronologies from the U/Th method or the tree ring method, a plateau in radiocarbon ages at the end of the Younger Dryas has been reported (Bard, 1990; Becker et al., 1991).

Other features of the model simulations are in disagreement with findings from geological records. Although there is a significant delay between meltwater input and a signature in the heat transport of the Atlantic in the model (up to 200 years in experiment MWF), this delay is definitely too small to explain

the observed delay of about 1000 years between meltwater peak and the onset of the Younger Dryas cold spell (Fairbanks, 1989). From the distribution of benthic δ13C, Sarnthein et al. (1994) conclude that there was still a significant production of upper NADW during the Younger Dryas. Hence the origin of the Younger Dryas is still an enigma.

6. Summary and conclusions

An idealized meltwater input peak with a total input corresponding to 13.4 m of global sea level change distributed over 500 years into the Labrador Sea turned out to be sufficient to suppress the formation of NADW for several hundred years. With a purely thermodynamic atmosphere model the system settles in a stable mode without any NADW formation. When a dynamic response of the atmosphere is permitted, this mode turns out to be slightly unstable, and the system slowly returns into a mode with NADW. Essentially, this behaviour is due to the erosion of the freshwater lens at the surface through increased upwelling in the GIN Sea and to a stronger export of the relatively fresh surface water by the intensification of the East Greenland current. The initially shallow convection deepens continuously, and the outflow of intermediate water both deepens and becomes stronger until finally the conveyor belt circulation resumes. During the periods with a collapsed conveyor belt, northward heat transport in the Atlantic is reduced by almost 80% to 0.2 PW. This leads to a strong cooling in the northern hemisphere with its center over the northern North Atlantic. The maximum cooling is delayed relative to the maximum of the meltwater input. The time span for the delay depends strongly on the location of the input. With a similar delay, NADW and AABW formation are out of phase, with an increase in AABW formation (and increased southward oceanic heat transport) occurring during periods of suppressed NADW formation.

The temporary collapse of the formation of NADW leads to a couple of clear signatures in geochemical tracers that can be derived from marine sediment cores: the water mass boundary between NADW and AABW shows a marked upward shift. This movement starts within less than 100 years after the collapse of NADW formation. The differences in radiocarbon ages between surface and deep (note: not bottom) Atlantic increase rapidly, at some locations the model simulations predict even a reversal of the deep radiocarbon chronology. When the system returns into modes with NADW, a rapid return to younger water with NADW characteristics can be found. In the atmosphere, Δ14C values increase by more than 12 ‰ during the meltwater event as a consequence of the reduced ventilation of the deep ocean. Thus, the radiocarbon chronology shows a rapidly gaining radiocarbon 'clock' at the early phases of the meltwater experiment and almost a standstill as soon as strong NADW formation resumes. In the surface ocean, changes in upwelling and mixing with deeper older water masses can cause local variations in the apparent radiocarbon chronology by more than 100 years compared to the atmospheric history. The exact size of these local deviations is certainly dependent on the details of the prescribed piston velocities.

At least with the assumptions about a constant δ18O of the net freshwaterflux forcing field, δ18O in the sea water gives a good qualitative estimate of the history of surface salinity as long as no sea ice effects are involved. But the relationship becomes less clear during periods of strong supply of meltwater. In the experiments presented here, errors were typically larger than 1 psu during periods of strong meltwater input. In the deep Atlantic, the meltwater effect can be detected as a slight reduction in the δ18O of sea water showing a recovery with the renewed arrival of NADW. This meltwater signal is obscured in the δ18Ocarb records of benthic foraminifera, since the AABW now filling the deep Atlantic is colder by more than 1°C, thus largely compensating for the meltwater effect. In most Atlantic locations, this

temperature effect is strong enough to reverse the sign of the signal in deep $\delta 18O_{carb}$.

Acknowledgements:

I appreciated discussions with and comments by Wally Broecker, Martin Heimann, Georg Hoffmann, and Ernst Maier-Reimer. Hanna Ogle helped to improve the English and Stephan Schultz made some of the plots. This work was in part funded by the German WOCE propram of the BMBF.

References:

Arakawa, A. and V.R. Lamb, 1977, Computational design of the basic processes of the UCLA General Circulation Model, Methods Comput. Phys., 17, 173-265.

Bard, E., B. Hamelin, R.G. Fairbanks, and A. Zindler, 1990, Calibration of the 14C timescale over the past 30,000 yeas using mass spectrometry U-Th ages from Barbados corals, Nature 345, 405-410.

Becker, B., B. Kromer, and P. Trimborn, 1991, A stable-isotope tree-ring timescale of the late glacial/holocene boundary, Nature 353, 647-649.

Bengtsson, L., K. Arpe, E. Roeckner, and U. Schulzweida, 1996, Climate predictability experiments with a general circulation model, Climate Dynamics (in press)

Boyle, E.A. and L. Keigwin, 1987, North Atlantic thermohaline circulation during the past 20,000 years linked to high-latitude surface temperature, Nature 330, 35-40.

Broecker, W.S. 1991, The Great ocean conveyor, Oceanography, 4, 79-89.

Broecker, W.S., M. Andree, W. Wolfli, H. Oeschger, G. Bonani, J. Kennett, and D. Peteet, 1988, The chronology of the last deglaciation: implications to the cause of the Younger Dryas event, Paleoceanography 3, 1-19.

Broecker, W.S., J.P. Kennett, B.P. Flower, J.T. Teller, S. Trumbore, G. Bonani, and W. Wolfli, 1989, Routing of meltwater from the Laurentide Ice Sheet during the Younger Dryas cold episode, Nature, 341, 318-321.

Bryan, F., 1986, High latitude salinity effects and interhemispheric thermohaline circulations, Nature, 323, 301-304.

Craig, H. and L.I. Gordon, 1965, Deuterium and oxygen 18 variations in the ocean and the marine atmosphere, In: E. Tongiorgi (ed.), Stable Isotopes in oceanographic studies and paleotemperatures, CNR, Pisa.

Dansgaard, W., J.W.C. White, and S.J. Johnsen, 1989, The abrupt termination of the Younger Dryas climate event, Nature 339, 532-534.

Duplessy, J.-C., L. Labeyrie, A. Juillet-Leclerc, F. Maitre, J. Duprat, M. Sarnthein, 1991, Surface salinity reconstruction of the North Atlantic Ocean during the last glacial maximum, Oceanologica Acta 14, 311-324.

Duplessy, J.C., L. Labeyrie, A. Juillet-Leclerc and J. Duprat, 1992, A new method to reconstruct sea surface salinitty: application to the North Atlantic Ocean during the Younger Dryas, in: E. Bard and W.S. Broecker (eds.) The Last Deglaciation: Absolute and Radiocarbon Chronologies, Springer-Verlag, Heidelberg, 201-217.

Fairbanks, R.G., 1989, A 17,000-year glacio-eustatic sea level record: Influence of glacial melting rates on the Younger Dryas event and deep-ocean circulation, Nature, 342, 637-642.

Hellermann, S. and M. Rosenstein, 1983, Normal monthly windstress over the World Ocean with error estimates, J. Phys. Oceanogr. 13, 1093-1104.

Imbrie, J., and N.G. Kipp, 1971, A new micropaleontological method for quantitative paleoclimatology: Application to a late Pleistocene Caribbean core, in: K.K. Turekian (ed.), The Late Cenozoic Glacial Ages, Yale Univ. Press, New Haven, Conn., 71-179.

Keigwin, L.D. and S.J. Leman, 1994, Deep circulation change linked to Heinrich event 1 and younger Dryas in a middepth North Atlantic core, Paleoceanography 9, 185-194.

Lehman, S.J., D.G. Wright and T.F. Stocker, 1993, Transport of freshwater into

the deep ocean by the conveyor, in: Ice in the climate system, edited by W.R. Peltier, pp. 187-209, Springer-Verlag.
Levitus, S., 1982, Climatological atlas of the World Ocean, NOAA Prof. Pap. 13, 173pp.
Liss, P.S. and L. Merlivat, 1986, Air Sea gas exchange rates: introduction and synthesis, in: P. Buat-Menard (ed.) The role of air-sea exchange in geochemical cycling, p. 113-127.
Maier-Reimer, E. and U. Mikolajewicz, 1989, Experiments with an OGCM on the cause of the Younger Dryas, Proc. JOA 1988, 87-99.
Maier-Reimer, E., U. Mikolajewicz and K. Hasselmann, 1993, Mean circulation of the LSG OGCM and its sensitivity to the thermohaline surface forcing, J. Phys. Oceanogr., 23, 731-757.
Manabe, S. and R.J. Stouffer, 1988, Two stable equilibria of a coupled ocean-atmosphere model, J. Clim., 1, 841-866.
Manabe, S. and R.J. Stouffer, 1995, Simulation of abrupt climate change induced by freshwater input to the North Atlantic Ocean, Nature, 378, 165-167.
Martinson, D.G. and C. Wamser, 1990, Ice drift and momentum exchange in winter Antarctic pack ice, J. Geophys. Res., 95, 1741-1755.
Mikolajewicz, U. and E. Maier-Reimer, 1994, Mixed boundary conditions in ocean general circulation models and their influence on the stability of the model's conveyor-belt, J. Geophys. Res., 99, 22633-22644.
North, G.R., J.G. Mengel and D.A. Short, 1983, Simple energy balance model resolving the seasons and the continents: Application to the astronomical theory of ice ages, J. Geophys. Res. 88, 6576-6586.
Preisendorfer, R.W., 1988, Principal Component Analysis in Meteorology and Oceanography, Develop. in Atmos. Sci. vol. 17. 425 pp., Elsevier, New York.
Roeckner, E., et al. , 1992, Simulation of the present-day climate with the ECHAM model: Impact of model physics and resolution, Max-Planck-Institut für Meteorologie, Report No. 93, Hamburg, 171 pp.
Rooth, C., 1982, Hydrology and ocean circulation. Prog. Oceanogr., 11, 131-149.
Sarnthein, M. et al., 1994, Changes in east Atlantic deepwater circulation over the last 30,000 years: Eight time slice reconstructions, Paleoceanography 9, 209-267.
Sarnthein, M. and R. Tiedemann, 1990, Younger Dryas-style cooling events at glacial terminations I-VI at ODP site 658: Associated benthic δ13C anomalies constrain meltwater hypothesis, Paleoceanography 6, 1041-1055.
Schiller, A., U. Mikolajewicz and R. Voss, 1996, The stability of the thermohaline circulation in a coupled ocean-atmosphere general circulation model, Climate Dynamics, subm.
Schmitz, W.J., 1995, On the interbasin-scale thermohaline circulation, Review of Geophysics 33, 151-173.
Stommel, H.H., 1961, Thermohaline convection with two stable regimes of flow, Tellus, XIII, 224-230.
Stuiver, M. and H.G. Östlund, 1980, GEOSECS Atlantic radiocarbon, Radiocarbon, 22, 1-24.
Toggweiler, J.R., K. Dixon and K. Bryan, 1989, Simulations of Radiocarbon in a coarse-resolution world ocean model. part I: Steady-state prebomb distributions, J. Geophys. Res. 94 (C6), 8217-8242.
Voss, R., R. Sausen and U. Cubasch, 1996, Periodically-synchronously coupled integrations with the atmosphere-ocean general circulation model ECHAM3/LSG, in preparation.
Wang, L., M. Sarnthein, J.-C. Duplessy, H. Erlenkeuser, S. Jung and U. Pflaumann, 1995, Paleo sea surface salinities in the low latitude atlantic: the δ18O record of Globigerinoides ruber (white), Paleoceanography 10, 749-761.
Zahn, R. and A.C. Mix, 1991, Benthic foraminiferal δ18O in the ocean's temperature-salinity-density field: constraints on ice age thermohaline circulation, Paleoceanography 6, 1-20.